

Research Article

Study on Failure Mechanism and Control Technology of Roadway Surrounding Rock under Complex Occurrence Coal Seam

Hai Wu ^{1,2}, Jiaren Chen,^{1,2} Xu Gao,³ Tao Ling,⁴ Xuan Zhang,^{1,2} and Qian Jia^{1,2}

¹School of Resources, Environment and Safety Engineering, Hunan University of Science and Technology, Xiangtan 411201, China

²Work Safety Key Lab on Prevention and Control of Gas and Roof Disasters for Southern Coal Mines, Hunan University of Science and Technology, Xiangtan 411201, China

³China Occupational Safety and Health Association, Beijing 100013, China

⁴Railway No. 5 Bureau Group First Engineering Co., Ltd., Changsha 411104, China

Correspondence should be addressed to Hai Wu; wuhai@hnust.edu.cn

Received 5 May 2022; Accepted 27 June 2022; Published 18 July 2022

Academic Editor: Dongjiang Pan

Copyright © 2022 Hai Wu et al. This is an open access article distributed under the Creative Commons Attribution License, which permits unrestricted use, distribution, and reproduction in any medium, provided the original work is properly cited.

Aiming at the characteristics of large deformation and long deformation time under the mining influence of the 2254 east floor roadway surrounding rock, which under the condition of complex coal occurrence in Jiahe Mine. Through the actual measurement, it is found that the mineral composition of the roadway surrounding rock is mainly siderite, and it also contains 9.52% of kaolinite minerals, and the surrounding rock is relatively weak. Through drilling and peeping, it is found that the roadway surrounding rock is mainly thin-layered, and a large number of fissures are developed in the surrounding rock near the surface of the roadway. Through the in situ stress test, it is concluded that the in situ stress field of Jiahe Mine is dominated by horizontal stress, the minimum principal stress is vertical principal stress, and the lateral pressure coefficient exceeds 2, causing serious damage to the two sides of the roadway. Using the gas drainage drilling data of the 2254 east floor roadway and using SketchUp and Rhino software, the complex geological occurrence model of the coal seam above the roadway was constructed, and on this basis, the FLAC3D numerical calculation model was constructed. The analysis results show that the plastic zone of the roadway surrounding rock is large, the bolt anchoring section is within the plastic zone, and the control effect on the deformation of the roadway surrounding rock is poor. Therefore, a comprehensive support method of “reserved deformation, anchor rod, metal mesh, shotcrete, grouting anchor cable, and full-section grouting” is proposed. The monitoring results of the surrounding rock deformation of the roadway 12 months after construction show that the support scheme can effectively control the deformation of the roadway surrounding rock. The research results provide a reference for the stability control of similar roadways.

1. Introduction

In recent years, my country's national economy has developed rapidly, and energy demand has remained high. In 2021, my country's total coal production will reach 4.13 billion tons, and the proportion of coal's primary energy will remain stable at more than 50% for a long time. Coal mines in southern China generally have complex occurrence conditions and poor mining conditions. Therefore, there are many factors affecting roadway deformation during the mining process, and the deformation mechanism is unclear. At present, scholars at home and abroad have carried out

certain research on roadway deformation and support under complex conditions. Chen et al. [1] believe that there is a difference in the original rock stress between the coal seam under complex geological conditions and the coal seam under ordinary conditions. Wang et al. [2] believed that the impact tendency of coal rock mass in complex geological occurrence environments is strong. Liang et al. [3] used three-dimensional microseismic monitoring technology to detect the microseismic activities inside the tunnel surrounding rock with complex geological conditions and high ground stress. Yanlin et al. [4] analyze the uncertainty, complexity, and diversity of geological bodies and enumerate the

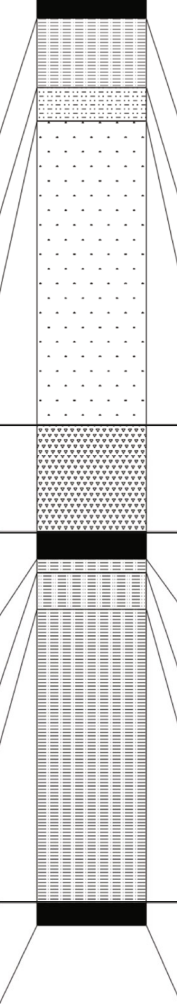
Layer number	Layer thickness (m)	Comprehensive histogram (1:500)	The name of the rock	Lithological description	Remark
1	$\frac{0.85}{0.80\sim 0.90}$		II coal	Black, weak metallic luster, pulverized coal, with only horizons seen in local areas.	2308 drilling data drawn
2	$\frac{2.66}{0\sim 3.96}$		Sandy mudstone	Gray-black, thin-layered, horizontal bedding, mixed with a small amount of siderite nodules, producing plant fossils.	
3	$\frac{1.29}{0\sim 2.9}$		Fine sandstone	Light gray, thinly layered, mixed with argillaceous and siderite bands, rich in white horizontal and microwave-like bedding.	
4	$\frac{28.5}{26.5\sim 31.31}$		Medium-grained sandstone	Gray-white, mainly medium-thick layers, with fine sandstone thin layers in the lower part. The sorting is general. The composition is mainly quartz, rich in muscovite flakes (layer enrichment), and feldspar is the second.	
5	$\frac{8.6}{0\sim 14.89}$		Siltstone	Dark gray to gray-white, thick layered, mainly composed of quartz, followed by feldspar, relatively loose, the upper part is dominated by cross-bedding, the middle and lower part is gently wave-like bedding, the layer contains mica flakes, chlorite and siderite.	
6	$\frac{1.45}{0.19\sim 4.4}$		V coal	Black, weak metallic luster, with shell-shaped fracture, light weight, is a semi-bright briquette mainly bright coal, mixed with mirror coal and dark coal strips.	
7	$\frac{0.22}{0\sim 0.88}$		Sandy mudstone	Gray-black, thin-layered, horizontal bedding, mixed with a small amount of siderite nodules, producing plant fossils.	
8	$\frac{0.96}{0\sim 3.87}$		Fine sandstone	Light gray, thinly layered, mixed with argillaceous and siderite bands, rich in white horizontal and microwave-like bedding.	
9	$\frac{27.87}{9.85\sim 36.35}$		Sandy mudstone	Dark gray, thin layered, horizontal bedding, containing plant fossils and fragmentary fossils, containing siderite nodules mixed with thin layers of siltstone, with a small amount of sea bean sprout fossils in the upper part.	
10	$\frac{0.80}{0\sim 2.15}$		Vi coal	Powdery, dark coal, occasionally mixed with gangue, only horizons in other areas.	

FIGURE 1: Comprehensive columnar diagram of roadway surrounding rock.



FIGURE 2: Bending deformation of roadway roof.

complex geological conditions that control the spatial form and physical distribution of geological bodies. Li et al. [5] constructed a multicoal seam logging interpretation model. Liang et al. [6] discussed the occurrence mechanism and key technologies for the prevention and control of coal-rock gas dynamic disasters in a magmatic rock occurrence

environment. Jiang et al. [7] studied the failure law of thin coal seams under complex conditions. Wang et al. [8] evaluated the stability of goaf with complex landforms and multiple coal seams. Zheng [9] studied the maximum cutting height of complex thick coal seam conditions. Lu et al. [10] believed that the plastic failure of complex coal bodies will



FIGURE 3: Rib deformation of roadway.

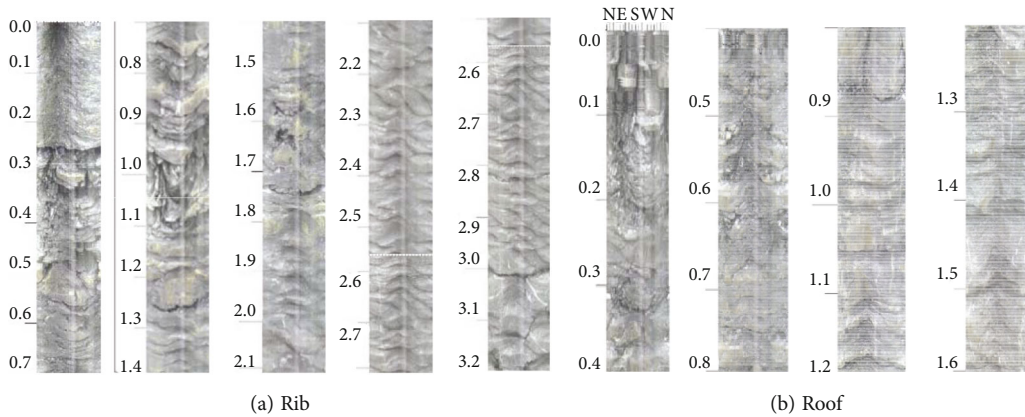


FIGURE 4: Peek view of borehole roadway surrounding rock.

TABLE 1: Horizontal and vertical stress data table.

Test hole number	Horizontal principal stress/MPa	Vertical principal stress/MPa	Lateral pressure coefficient
ZL-1	8.6	6.5	1.3
ZL-2	9.8	5.4	1.8
Mean	9.2	6.0	1.5

lead to a large amount of gas release. Wang et al. [11] studied the factors of back-arching instability of roadway floor under complex conditions. Yuan et al. [12] believed that the deformation symmetry of the roadway surrounding rock is poor under complex conditions, so asymmetric support is a better choice. Oparin et al. [13] introduced the comprehensive method and results of deformation wave monitoring of temporary lining of railway tunnels under complex geological conditions in southern Western Siberia. Wu et al. [14] discussed the influence of mud parameters and drilling speed on the quality of hole formation under complex geological conditions and obtained effective drilling speed and economical and reasonable mud parameters. To simulate the seismic performance of subway tunnels under complex geological conditions excited by oblique-incidence earthquakes, Gao et al. [15] established an overall numerical model of subway tunnels and foundations. Jianbing et al. [16] established a local elastic foundation model, studied the mechan-

ical properties of the tunnel filling karst effect on the lining structure, and derived the calculation formulas for the displacement, bending moment, and shear force of the equivalent beam. Li [17] used the numerical simulation method to reveal the variation law of borehole stress after coal seam cutting through drilling and bedding drilling. Liaojun et al. [18] proposed a stability analysis method that can reflect the complex geological structure of the dam foundation. To realize safe and efficient mining in thin coal seams with complex geological conditions, Tongbin et al. [19] proposed an innovative pressure-regulated mining method. Yu et al. [20, 21] clarified the main points of support for weak semi-coal rock roadways and proposed the idea of strengthening the lateral support of surrounding rock and improving the overall mechanical strength of such roadways. Wang et al. [22–24] found that the tunnel floor heave was inversely proportional to the strength of the two coal bodies and proposed that the deformation space should be reserved in advance, and the supporting structure should be adapted to it. Cui et al. [25] studied the deformation and stress distribution law of mining roadway and obtained the influence law of mining stress. The above studies have proposed the failure mechanism and stability control of the roadway surrounding rock under the condition of complex occurrence of coal gobs, but the roadway surrounding rock of the southern coal mine is weak, and the coal body occurrence conditions are complex. The existing roadway surrounding rock control measures still have certain limitations and cannot fully guide

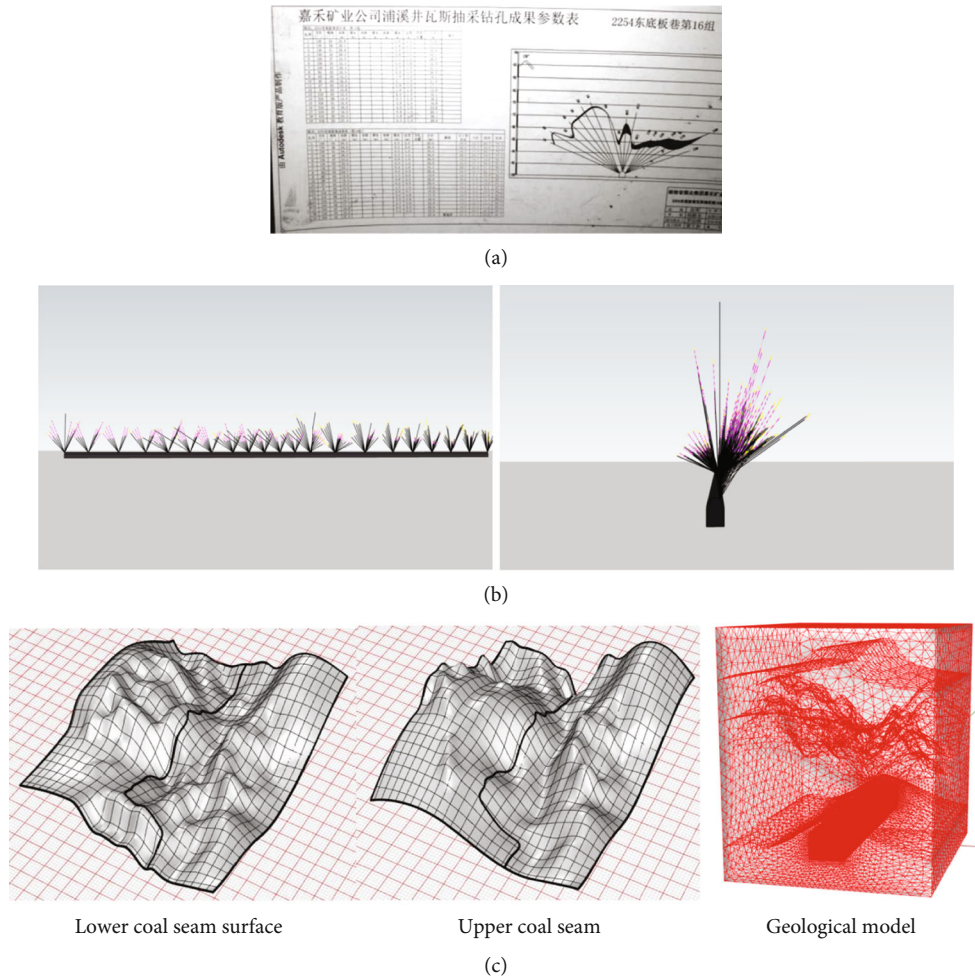


FIGURE 5: (a) Gas drainage drilling results of 15 groups in the 2254 east floor roadway. (b) Each borehole rock mass and coal seam foundation model. (c) Coal seam fitting surface and geological model.

the stability control of the same type of roadway surrounding rock. Therefore, this paper takes the 2254 east floor roadway of Puxi Well as the object, analyzes the deformation mechanism of floor roadway under the condition of complex coal body, and proposes a comprehensive support method. This method is suitable for most of the same type of roadway and can effectively make up for the limitations of the existing roadway surrounding rock stability control measures.

2. Engineering Background

The Puxi mine of Jiahe Mining Company is located in the northeast of Jiahe County. The geological conditions of the rock formations are complex. The structures are mainly divided into three groups: north-south, north-west, and east-west. The overall mine rock formation is an undulating and sinuous syncline-anticline composite structure. The 2254 working face starts from the south wing of the 22 mining area -80 horizontal transport stone gate, north to the 22 mining area F63 fault boundary, east to the 11511 working face that has been mined, and west to the 22 mining area -105 horizontal gas drainage control area edge. Excavating along the V coal floor, the coal seam structure is complex

and bumpy and can be exploited locally. The comprehensive histogram of this area is shown in Figure 1. 2254 east floor roadway has a semicircular arch structure with a cross-section of 2600 mm × 2700 mm and adopts the form of bolt mesh spraying support, and the length of the bolt is 1800 mm.

3. Analysis of Deformation and Failure Characteristics of Roadway Surrounding Rock

3.1. Analysis of Surface Failure Characteristics of Roadway Surrounding Rock. Under the original support scheme of the 2254 east floor roadway, the roof bends and sinks seriously, the local shotcrete layer falls off, the layered surrounding rock is broken, and the separation layer between the surrounding rock layers is common, and the anchor bolt is suspended, as shown in Figure 2.

The two sides of the roadway are asymmetrically deformed, the left side of the roadway is relatively stable, and the right side of the roadway shows serious intrusion, chipping, cracking, and other phenomena. As shown in

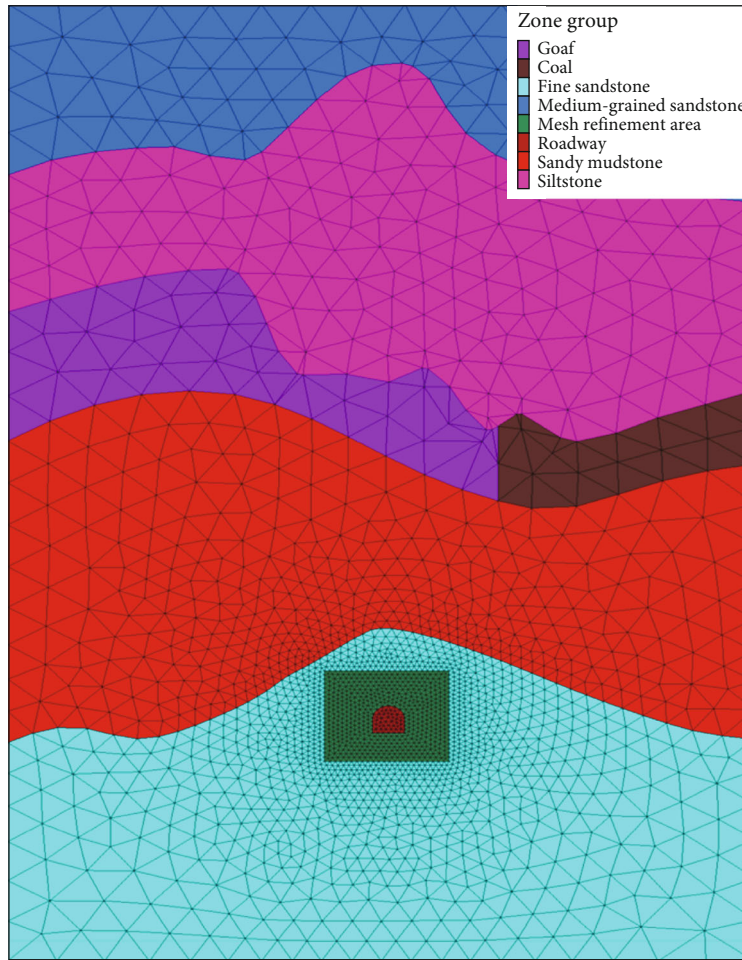


FIGURE 6: Numerical simulation model.

TABLE 2: Numerical calculation parameters.

Surrounding rock type	Bulk modulus/ MPa	Shear modulus/ MPa	Rock mass density/ (kg•m ³)	Internal friction angle/(°)	Cohesive force/ MPa
Medium-grained sandstone	2100	1.32	2750	32	3.50
Siltstone	3200	2.70	2650	30	2.30
Coal	270	0.16	2235	22	0.75
Sandy mudstone	900	0.01	2600	25	2.95

Figure 3, the “S”-shaped extrusion and bending deformation occurred in the surrounding rock, which led to the collapse of the right side roadway and the exposed bolts, which seriously affected the normal passage of the roadway.

3.2. Analysis of the Development of Fissures in Road Surrounding Rock. A borehole peeping instrument is used to record the internal damage of the roadway roof and the surrounding rock of the side. The peeping results of the surrounding rock at the side of the roadway show that (Figure 4(a)) there are obviously broken zones of surrounding rock within two ranges of 0.3 m-0.4 m and 0.8 m-1.1 m

from the surface of the roadway side. Single cracks developed at 0.5 m and 1.3 m. There is a cavity at 1.6 m-1.7 m, the whole is continuous at 1.8 m-3.0 m, and cracks develop at 3.0 m-3.2 m.

When the tunnel roof was drilled and peeped, there was a broken rock zone at 1.6 m of the drilling position, so only the surrounding rock data within 1.6 m of the roof was obtained (Figure 4(b)). The results show that there are a lot of cracks in the surrounding rock at 0.1 m~0.6 m. The vertical and horizontal cracks can be seen at 0.8 m~0.9 m, the integrity of the surrounding rock within 0.9 m~1.1 m is good, and there are cracks at 1.2 m, 1.4 m, and 1.5 m.

3.3. Mineral Composition Analysis of Roadway Surrounding Rock. To further understand the characteristics of the roadway surrounding rock, we used an X-ray diffractometer to analyze its composition. The analysis results show that the mineral composition of the roadway surrounding rock is mainly siderite, with a content of 51.34%, followed by quartz 15.82, mica (15.38%), and kaolinite (9.52%), in addition to a small amount of anatase and feldspar. Among them, the nature of siderite is relatively unstable, and it is easy to be weathered or hydrolyzed in contact with air. Due to its special structure, the mica will become very fine debris under the influence of pressure or weathering. Kaolinite with a larger content is less hard, often in the form of soil or lumps. If the environment is humid or water enters, it will easily become ooze or even disintegrate.

3.4. Ground Stress Test. To grasp the stress environment of the roadway surrounding rock, we carried out the in situ stress test on the coal mine. The test results are shown in Table 1.

The test results show that the maximum horizontal stress in the mining area is 1.8 times the vertical stress, and the horizontal principal stress direction is perpendicular to the roadway axis.

4. Stability Simulation Analysis of Floor Roadway and Optimization of Support Parameters

4.1. Building the Geological Model. In order to grasp the occurrence of the coal seam above the 2254 east floor roadway, using the parameter map of the gas drainage drilling results in the roadway (Figure 5(a)), and using SketchUp combined with Rhino software, the coal seam fitting lower surface and upper surface were established.

Firstly, the SketchUp software is used to determine the drilling angle according to the azimuth and inclination in each group of extraction drilling holes. Then, use the black curve, the red dotted line, and the yellow curve to draw the length of the rock mass, coal seam, and overtop, respectively, at the drilling position, so as to construct the rock mass and coal seam foundation model of each drilling hole above the roadway, as shown in Figure 5(b).

The coal length curves made by different hole numbers of each borehole are connected to establish the coal seam profile above each group of borehole roadways. Import the basic model built by SketchUp into Rhino, determine the relative position and unit of the imported model, and fit all the lower and upper surface points to the lower surface and upper surface of the coal seam. In order to make the surface closer to the point cloud, try to let the fitted surface pass more feature points, and set the most suitable fitting parameters through continuous debugging, so as to obtain the final model, as shown in Figure 5(c).

4.2. Numerical Simulation Model and Related Calculation Parameters. The geological model established by Rhino was imported into FLAC3D, and the situation of the 2254 east floor roadway affected by the occurrence of complex coal

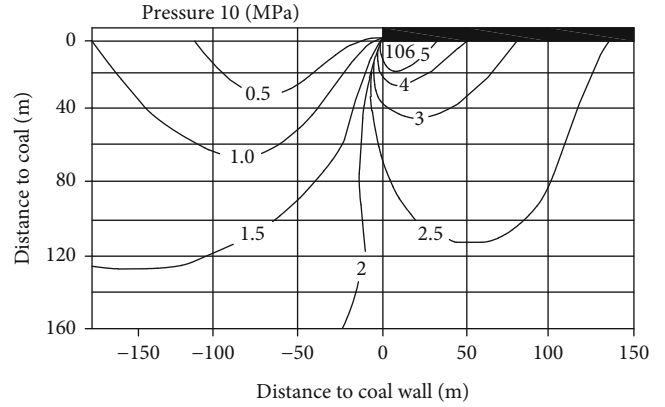


FIGURE 7: Contour map of maximum principal stress distribution of floor rock stratum.

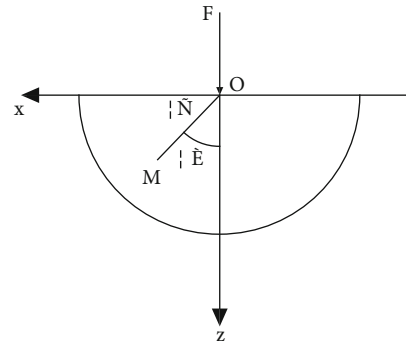


FIGURE 8: Semi-infinite planar body of floor rock under the action of load F .

seams was analyzed. According to the geological structure obtained from field exploration, the model is divided into six layers from top to bottom: medium-grained sandstone, siltstone, coal, sandy mudstone, roadway, and argillaceous sandstone. The dimension of the straight wall semicircular arch roadway is 2600 mm \times 2700 mm (width \times height). The roadway was originally supported by anchors, nets, and spray. The anchor rod is $\Phi 16 \times 1800$ mm full-threaded steel, and the anchor rod is anchored by a resin coil. The model adopts the Cartesian coordinate system, and the generated mesh is divided into 670,020 elements and 114,705 nodes. At the same time, to ensure more accurate simulation, the surrounding rock within 6 m around the roadway is encrypted, as shown in Figure 6.

Model boundary conditions: lower boundary: displacement is zero; left, right, front, and rear boundaries: horizontal displacement is zero; upper boundary: free boundary, vertical stress 6 MPa; model lateral pressure coefficient is set to 2. The model adopts the Mohr-Coulomb yield criterion. The mechanical parameters of the surrounding rock are shown in Table 2.

4.3. Mechanical Analysis of the Stability of Floor Roadway under the Influence of Upper Working Face Mining. To study the stability of 2254 east floor roadway under the influence

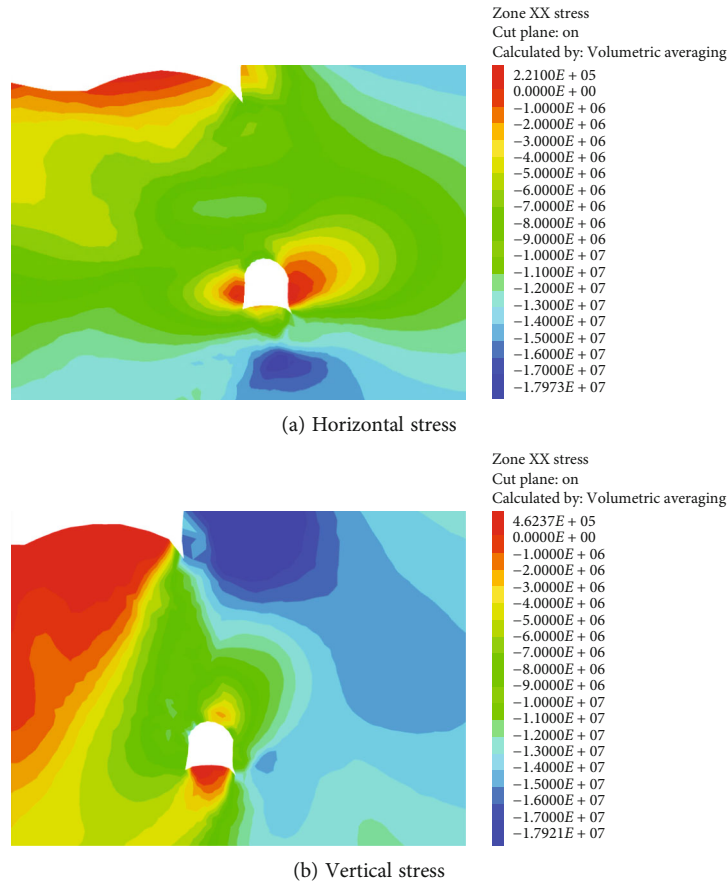


FIGURE 9: Cloud map of horizontal stress and vertical stress distribution of roadway under the influence of mining.

of working face mining, we must first understand the distribution and transmission law of lateral support pressure on the working face floor. By referring to the literature [26], the maximum principal stress transfer law of the working face was obtained, and the contour map of the maximum principal stress distribution of the floor strata was obtained, as shown in Figure 7.

Mining of the coal seam above the floor roadway leads to a regular transfer of the maximum principal stress of the rock formation. The main influencing factors include the vertical distance between the roadway and the upper working face and the horizontal distance between the coal wall edge of the roadway working face. Therefore, after the floor roadway is mined in complex coal seams, the stress distribution of the floor strata in the working face is closely related to the deployment position of the roadway. The difference in the spatial position between the goaf and the roadway makes the stress increase coefficient of the floor roadway vary greatly. According to the elastic mechanics' analysis, the transfer law of the stress generated during the mining of the working face in the floor rock can be obtained.

As shown in Figure 8, the floor rock formation at the boundary of the gob is regarded as a semi-infinite plane body. Under the action of the concentrated load F along the positive direction of Z in the figure, the polar coordinate

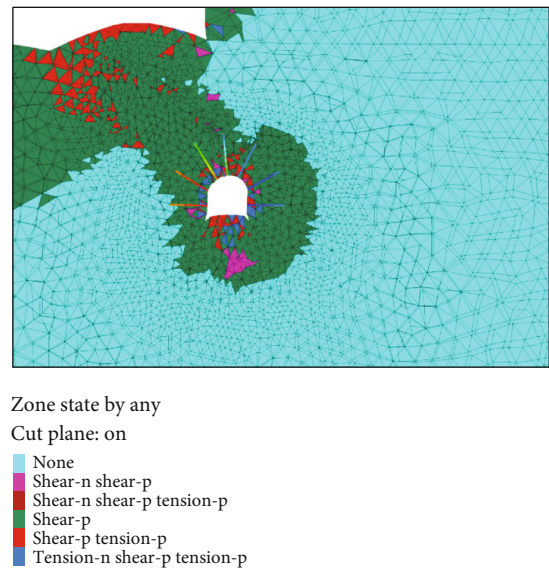


FIGURE 10: Distribution of plastic zone of the roadway under the influence of mining.

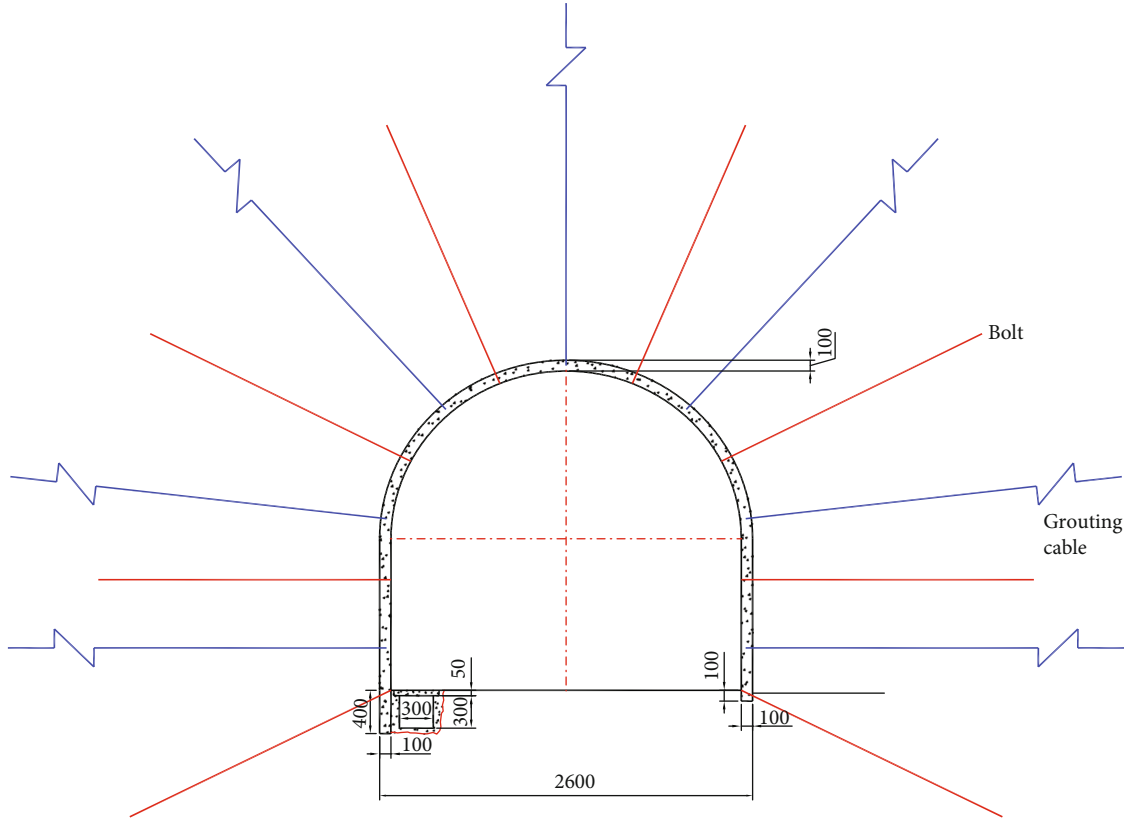


FIGURE 11: Anchor cable support section view.

expression of the mining stress at any position $M(\rho, \theta)$ in the floor stratum is:

$$\sigma_z = \frac{-2F \cos^3 \theta}{\pi \rho}, \quad (1)$$

$$\sigma_x = \frac{-2F \sin^2 \theta \cos \theta}{\pi \rho}, \quad (2)$$

$$\tau_{xz} = \frac{-2F \sin \theta \cos^2 \theta}{\pi \rho}. \quad (3)$$

In the formula, σ_x , σ_z , and τ_{xz} represent the stress components in three directions, respectively, which are converted into a rectangular coordinate system and expressed as:

$$\sigma_z = \frac{-2F}{\pi} \frac{x^3}{(x^2 + y^2)^2}, \quad (4)$$

$$\sigma_x = \frac{-2F}{\pi} \frac{xy^2}{(x^2 + y^2)^2}. \quad (5)$$

Based on the above analysis, it can be concluded that the maximum vertical stress generated by mining is distributed on the lower axis of the load center, which is negatively related to the depth of the rock mass, that is, the smaller the depth, the greater the stress. At the same time, the closer

to the axis, the greater the stress, and the easier it is for the surrounding rock to enter the plastic failure state.

4.4. Stability Simulation Analysis of 2254 East Floor Roadway Affected by Upper Working Face Mining. As shown in Figure 9, after the working face is mined, the original stress balance state of the surrounding rock is broken, and the gravity of the overlying rock layer in the goaf is transferred to the front of the working face in the direction of the strike to form an advanced support pressure. In the direction of inclination, the pressure is transferred to both sides of the working face to form the support pressure on both sides of the working face. A certain stress-increasing area is formed in the bottom plate of the working face.

Figure 9(a) shows that the horizontal stress distribution on both sides is different, the right side has a large deformation stress reduction area with a depth of about 2.4 m, and the affected area of the right side is about 1.5 m. Figure 9(b) shows that the right side of the roadway with the vertical stress floor forms a stress concentration area, and at the same time, a deformation stress reduction area appears on the roof on the right side of the roadway.

Figure 10 shows that after the mining effect, the plastic zone in the roadway surrounding rock is large, and the plastic zone is asymmetrically distributed. The width of the surrounding rock plastic zone on the right side of the roadway is 3.8 m, the depth of the bottom plastic zone is 3.2 m, the depth of the roof plastic zone is 2.1 m, and the minimum plastic zone on the left side is 1.8 m. The depth of the plastic

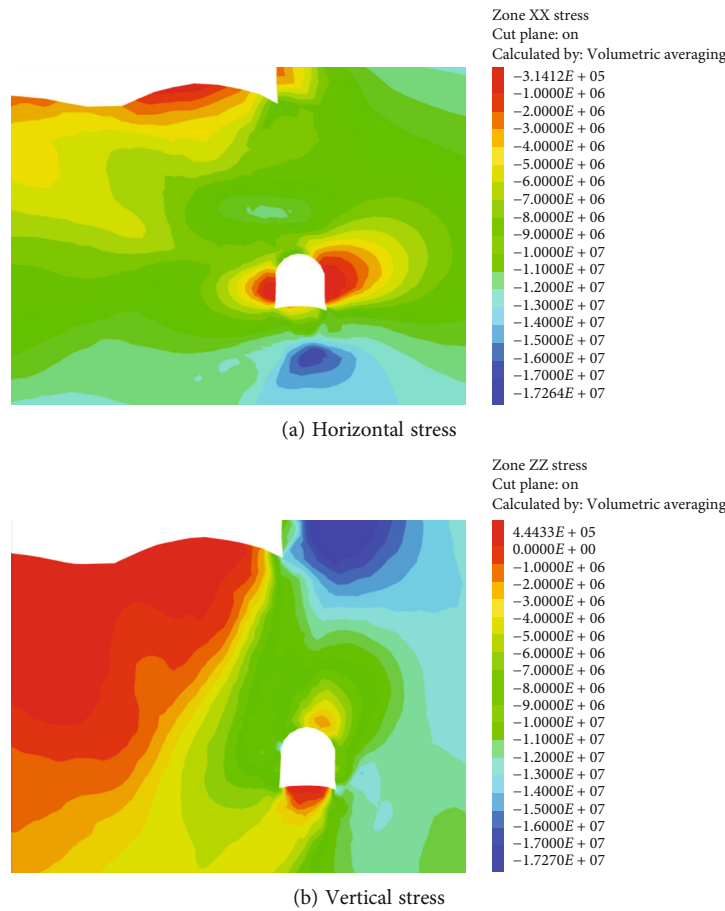


FIGURE 12: Optimize the horizontal stress and vertical stress distribution cloud chart after the optimization of the roadway.

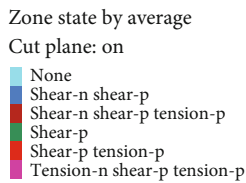
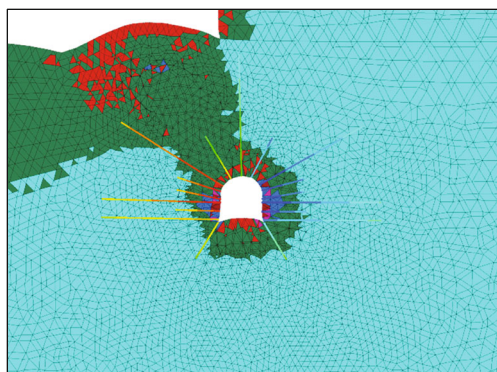


FIGURE 13: Distribution of plastic zone of the roadway under optimization scheme.

zone exceeds the length of the bolt, the effect of bolt support is weakened, and the deformation of the roadway surrounding rock cannot be effectively controlled.



FIGURE 14: Construction layout of the new scheme.

To sum up, after the upper working face of the roadway is mined, due to the increase of support pressure caused by mining, the original support scheme cannot control the stability of the floor roadway surrounding rock.

4.5. 2254 East Floor Roadway Improvement Support Scheme Design and Effect Simulation Analysis. Based on the above analysis, a comprehensive support method of “reserved deformation, anchor rod, metal mesh, shotcrete, grouting anchor cable, and full-section grouting” is proposed for the entire roadway section. Ensure the overall stability of the 2254 east floor roadway and prevent the large deformation

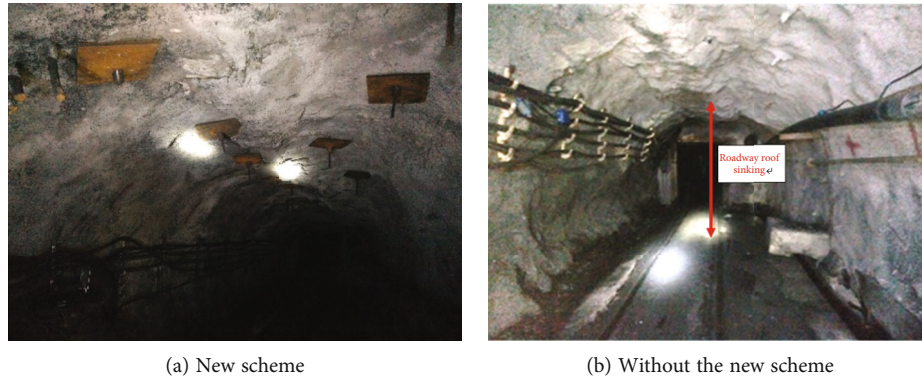


FIGURE 15: Comparison picture of deformation of roadway.

of its surrounding rock from affecting the normal production of the mine.

As shown in Figure 11, the anchor rod is made of BHRB500 $\Phi 22\text{mm} \times 2200\text{mm}$ left-handed rebar without longitudinal reinforcement. Each anchor uses 2 rolls of K2330 resin anchoring agent, the anchoring force is not less than 70 kN, the row spacing between the anchors is 700 mm \times 700 mm, the metal mesh is $\Phi 6\text{mm}$, the grid is 100 \times 100 mm, and the specification is 1000 mm \times 800 mm. There must be anchors where the metal mesh joins the stubble and is close to the rock surface, and the length of the stubble between the meshes is not less than 100 mm. The thickness of sprayed concrete is 100 mm, and the strength is C20. Using a steel plate tray, it is made into a square with a side length of 150 mm and a thickness of 8 mm.

The anchor cable adopts a grouting anchor cable with $\Phi 21\text{mm} \times 6100\text{mm}$, and the distance and discharge are 1200 \times 1400 mm. The end of the anchor is anchoring the resin, and the length of the anchor is 1500 mm. Each anchor cable uses 5 rolls of Z2850 resin rolls, and the anchoring power is not less than 100 kN. The anchor tray uses a compressed pad device, which is superimposed from two pads. The specifications are 350 mm \times 350 mm \times 10 mm and 150 mm \times 150 mm \times 10 mm square pads. The large pads are inside and the small pads are outside.

Select the roadway section of the vertical height of the working surface to 6.4 m as the research object. From the perspective of the stress concentration of the roadway surrounding rock, the development characteristics of the plastic area, the bottom plate of the lane roads, and the two groups of fenced rock displacement comparison the comparison of several aspects, the support effect of the optimization scheme is analyzed.

As shown in Figure 12, after the optimization support scheme is adopted, the peak stress peak of the surrounding rock level X is reduced compared with the original scheme. The distribution of horizontal stress on the sides of the surrounding rock is still asymmetric. The right side of the lane road is still greater than the left. The distribution of vertical stress is still the deformation stress release area on the right side of the top plate. In general, the stress peak value has a certain decrease than the original plan, which improves the overall stability of the surrounding rock.

It can be seen from Figure 13 that after the optimization scheme is adopted, the degree of asymmetric distribution of the plastic zone of the roadway surrounding rock is reduced. Among them, the width of the surrounding rock plastic zone on the right side of the roadway is reduced to 2.1 m, and the depth of the bottom plastic zone is reduced to 1.85 m. At the same time, in the improved support scheme, the length of the bolt is increased to 2200 mm, and the anchoring sections of the bolt and the cable are located in the elastic zone of the surrounding rock outside the plastic zone of the surrounding rock.

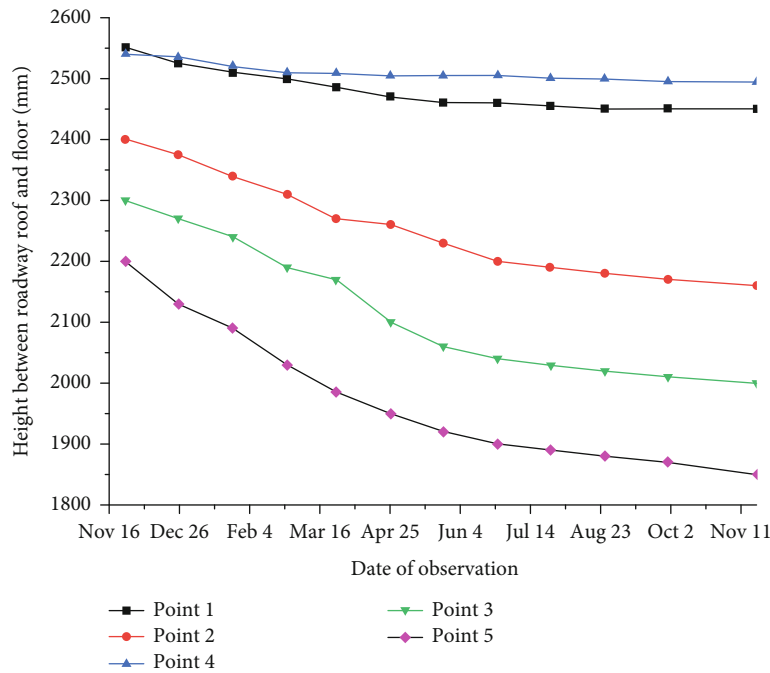
5. Analysis and Evaluation of Measured Data of Roadway Deformation in New and Old Schemes

The new scheme was adopted for construction in 2254 east floor roadway. The construction layout is shown in Figure 14. Observation points for the surface displacement of the roadway surrounding rock are set up within and outside the construction scope for data observation.

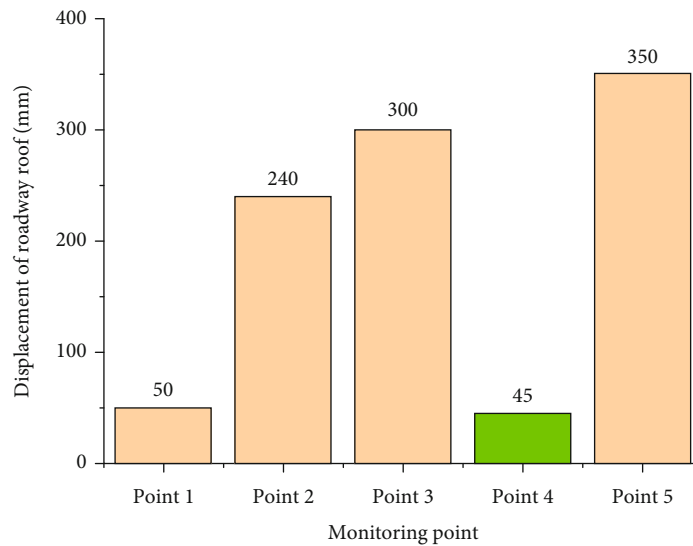
5.1. Observation Effect Analysis. The deformation of the roadway surrounding rock (the height of the roof and the floor and the width of the two sides) has been observed for one year. Figure 15(a) is the roadway diagram after the construction of the new scheme, and Figure 15(b) is the roadway deformation diagram without the implementation of the new scheme.

The following is a comparison chart of the height changes of the roof and floor at different monitoring points of the old and new schemes.

Figures 16(a) and 16(b) show that under the impact of mining, the top board of different observations has a certain degree of sinking. Point 4 (the construction section of the new plan) has the smallest sinking volume, and the height of the top board drops from the original 2540 mm to 2495 mm, a decrease of 45 mm. Point 5 (old plan construction section): the height of the top board dropped from the original 2200 mm to 1850 mm, the largest sinking volume, reaching 350 mm. The height of the top board of point 3 (the construction section of the old plan) dropped from 2300 mm to 2000 mm, sinking 300 mm. Point 2 (old plan



(a)

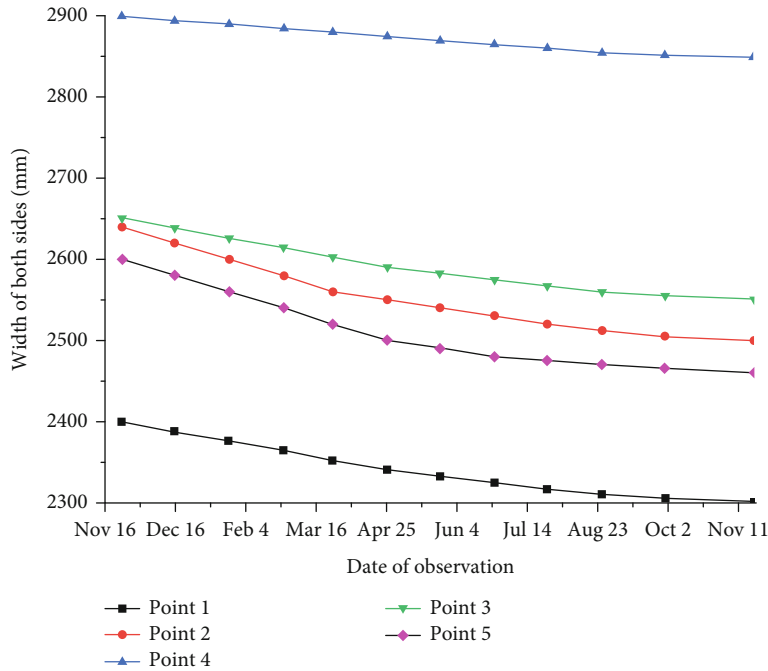


(b)

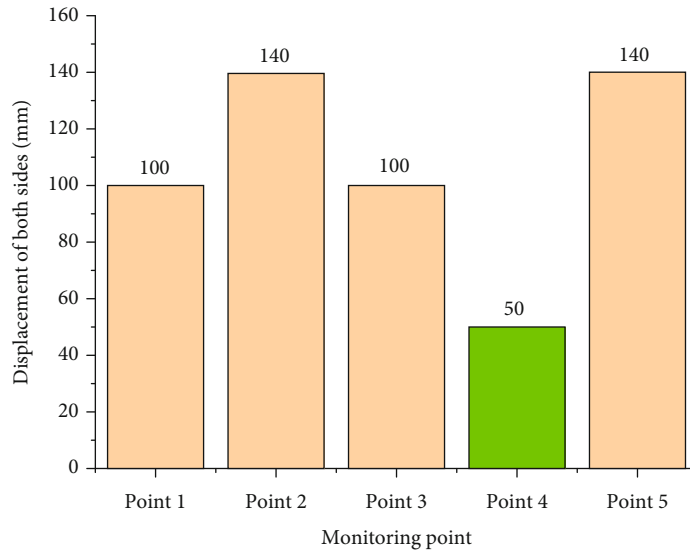
FIGURE 16: (a) Line chart of roadway roof and floor height change. (b) Column chart of roadway roof subsidence at different monitoring points.

construction section): top plate height dropped from 2400 mm to 2160 mm, sinking 240 mm. The height of the roadway at points 3 and 5 can no longer meet the normal walking needs. Pedestrians need to bow their heads to prevent head-butting. In addition, the roof height of no. 1 point (construction section of the old scheme, which is also located in the bottom plate of the goaf) is relatively small, from the original 2550 to 2450 mm, and the subsidence height is only 100 mm. Therefore, the support parameters should be further optimized for the roadway roof surrounding rock, especially the observation points 3 and 5.

5.2. Analysis of Observation Effect on Both Sides of the Roadway. The monitoring data (Figure 17) show that, under the influence of mining stress, the width on both sides of different monitoring points decreases to a certain extent. Point 4 (the construction section of the new scheme) has the smallest reduction in the width on both sides, from the original 2900 mm to 2850 mm, a reduction of 50 mm. Point 5 (construction section of the old scheme) was reduced from the original 2600 mm to 2460 mm, a reduction of 140 mm. Point 2 (construction section of the old scheme) has been reduced from the original 2640 mm to 2500 mm, a reduction of



(a)



(b)

FIGURE 17: (a) Line chart of the height change of the two sides of the roadway. (b) The bar chart of the height change of the two sides of the roadway.

140 mm. The no. 1 point (the construction section of the old scheme, which is also located in the bottom plate of the goaf) has been reduced from the original 2400 mm to 2300 mm, a reduction of 100 mm. No. 3 (the construction section of the old scheme): the width of the two gangs has been reduced from the original 2650 mm to 2550 mm, a reduction of 100 mm. Observation data show that the height of the top and bottom plates and the width of both sides of the roadway are significantly reduced after the new scheme is adopted, indicating that the new scheme can effectively control the deformation of the roadway.

6. Conclusion

- (1) In situ stress test results show that the roadway surrounding rock is dominated by horizontal stress, and the maximum horizontal principal stress is perpendicular to the axial direction of the roadway, resulting in stress concentration in the roadway surrounding rock. At the same time, the surrounding rock composition of the roadway includes 9.52% kaolinite, 4.75% chlorite, 51.34% siderite, 15.38% mica, and other minerals, resulting in the relatively weak

surrounding rock. It was found that the surrounding rock was damaged in the “M” type. At the same time, the drilling peek showed that there were a large number of cracks in the surrounding rock surface of the roadway within a range of 1.7 m

- (2) Aiming at the complex occurrence of coal seams, a model was built using SketchUp combined with Rhino software and then imported into Flac 3D for calculation. The calculation results show that under the original scheme, the plastic zone of the roadway surrounding rock has a large development range, and the bolt is in the plastic zone, which cannot effectively control the deformation of the roadway
- (3) A comprehensive support method of “reserved deformation, anchor rod, metal mesh, shotcrete, grouting anchor cable, and full-section grouting” is proposed for the 2254 east floor roadway, and numerical simulation is carried out. The simulation results show that under the new scheme, the approaching amount of the two sides of the roadway, the subsidence amount of the roof, and the bottom slump are greatly reduced
- (4) The monitoring comparison of the deformation data of the roadway surrounding rock after the old and new support schemes shows that the deformation of the roadway roof and floor heights (45 mm) under the new scheme is significantly smaller than the maximum deformation (350 mm) of the old scheme. Under the new scheme, the deformation of the width of the two sides of the roadway (50 mm) is significantly smaller than the maximum deformation (140 mm) of the old scheme. The new scheme can meet the needs of normal work, and the overall support effect is good

Data Availability

Data is available on request due to privacy restrictions.

Conflicts of Interest

The authors declare that there are no conflicts of interest regarding the publication of this article.

Acknowledgments

This research was funded by the National Natural Science Foundation of China, grant numbers 52074117 and 51774133.

References

- [1] T. Chen, B. Liang, W. Sun, and F. Zhao, “Research on pressure distribution regularity of complicatedly geologic CBM reservoir with multi-well exploitation,” *Journal of China Coal Society*, vol. 36, no. 4, pp. 603–608, 2011.
- [2] H. Wang, Y. Jiang, D. Deng, D. Zhang, J. Lv, and X. Zeng, “Investigation on the inducing factors of coal bursts under complicated geological environment in Yima mining area,” *Chinese Journal of Rock Mechanics and Engineering*, vol. 36, Supplement 2, pp. 4085–4092, 2017.
- [3] Z. Liang, R. Xue, N. Xu, and W. Li, “Characterizing rockbursts and analysis on frequency-spectrum evolutionary law of rockburst precursor based on microseismic monitoring,” *Tunneling and Underground Space Technology*, vol. 105, article 103564, 2020.
- [4] S. Yanlin, A. Zheng, Y. He, and X. Keyan, “3D geological modeling and its application under complex geological conditions,” *Procedia Engineering*, vol. 12, pp. 41–46, 2011.
- [5] C. Li, Z. Yang, H. Sun et al., “Construction of a logging interpretation model for coal structure from multi-coal seams area,” *Journal of China Coal Society*, vol. 45, no. 2, pp. 721–730, 2020.
- [6] W. Liang, H. Guo, Y. Cheng et al., “Abnormal coal seam gas occurrence characteristics and the dynamic disaster control technologies in the magmatic rock intrusion area,” *Journal of China Coal Society*, vol. 47, no. 3, pp. 1244–1259, 2022.
- [7] J. Jiang, J. Dai, H. Li, and Q. Hua, “Failure law and application of complex structure thin coal seam mining face,” *Journal of China Coal Society*, vol. 38, no. 11, pp. 1912–1916, 2013.
- [8] J. Wang, S. Wu, C. Ding, Y. Zhang, and G. Cai, “Stability evaluation of mine goaf with multi-coal seams and complex landform,” *Journal of China Coal Society*, vol. 34, no. 4, pp. 466–471, 2009.
- [9] J. Zheng, “Studying on coal mining method of stope face with complex thickness coal seam,” *Coal Mining Technology*, vol. 23, no. 3, pp. 25–29, 2018.
- [10] S. Lu, Y. Zhang, Z. Sa, and J. Liu, “Criterion of plastic failure and outburst energy instability of soft and hard composite coal,” *Journal of Mining & Safety Engineering*, vol. 36, no. 3, pp. 583–592, 2019.
- [11] C. Wang, Y. Wu, and X. Huang, “Mechanism of floor failure of roadway supported by inverted arch under complicated surrounding rocks and its control,” *Journal of Mining & Safety Engineering*, vol. 36, no. 5, pp. 959–967, 2019.
- [12] C. Yuan, H. Yin, L. Fan, and W. Tan, “Evaluation and analysis of supporting effect of roadway in complex conditions,” *Mineral Engineering Research*, vol. 35, no. 2, pp. 22–31, 2020.
- [13] V. N. Oparin, V. F. Yushkin, G. N. Polyankin, A. N. Grishin, A. O. Kuznetsov, and D. E. Rublev, “Geomechanical monitoring of temporal lining in railway tunneling in complex geological conditions,” *Journal of Mining Science*, vol. 51, no. 4, pp. 839–859, 2015.
- [14] Y. H. Wu, Z. Zhou, W. Q. Chen, S. Y. Liu, B. C. Zhang, and H. F. Huang, “Research on construction technology of cast-in-situ bored pile under complex geological conditions,” *IOP Conference Series: Earth and Environmental Science*, vol. 510, no. 5, article 052089, 2020.
- [15] X. Gao, P. Duan, and S. Duan, “Simulated seismic response analysis of subway tunnels under complex geological conditions of obliquely incident seismic SV waves,” *Arabian Journal of Geosciences*, vol. 14, no. 11, 2021.
- [16] L. Jianbing, L. Xulong, Y. He, F. Helin, and Y. Yingmei, “Analytical analyses of the effect of filled karst cavern on tunnel lining structure under complex geological conditions,” *AIP Advances*, vol. 9, no. 3, article 035148, 2019.
- [17] C. Li, “Experimental study via dynamic prediction model on high pressure hydraulic slotting and high efficiency gas

- drainage technology under complex geological conditions,” *Journal of Physics: Conference Series*, vol. 1769, no. 1, article 012021, 2021.
- [18] Z. Liaojun, T. Ma, Z. Hanyun, C. Dongsheng, and C. Piero, “Dynamic stability discrimination method for concrete dam under complex geological conditions,” *Mathematical Problems in Engineering*, vol. 2019, Article ID 3702712, 16 pages, 2019.
- [19] Z. Tongbin, Z. Zhenyu, Y. Tan, S. Chengzhong, W. Ping, and L. Quan, “An innovative approach to thin coal seam mining of complex geological conditions by pressure regulation,” *International Journal of Rock Mechanics and Mining Sciences*, vol. 71, pp. 249–257, 2014.
- [20] W. Yu, G. Wu, H. Liu et al., “Deformation characteristics and stability control of soft coal-rock mining roadway in thin coal seam,” *Journal of China Coal Society*, vol. 43, no. 10, pp. 2668–2678, 2018.
- [21] Y. Weijian, F. Tao, W. Weijun et al., “Support problems and solutions of roadway surrounding rock for thin coal seams under complex conditions in southern China,” *Journal of China Coal Society*, vol. 40, no. 10, pp. 2370–2379, 2015.
- [22] W. Wang and T. Feng, “Study on mechanism of reinforcing sides to control floor heave of extraction opening,” *Chinese Journal of Rock Mechanics and Mining Sciences*, vol. 5, pp. 808–811, 2005.
- [23] W. J. Wang, C. Yuan, W. J. Yu et al., “Control technology of reserved surrounding rock deformation in deep roadway under high stress,” *Journal of China Coal Society*, vol. 41, no. 9, pp. 2156–2164, 2016.
- [24] W. Wang, S. Li, and G. Ouyang, “Study on technique and test of surrounding rock control of DEEP shaft coal roadway,” *Chinese Journal of Rock Mechanics and Mining Sciences*, vol. 10, pp. 2102–2107, 2006.
- [25] J. Cui, W. Wang, Q. Jia, G. Peng, H. Wu, and P. Wang, “Measurement and analysis of roadway deformation and stress under mining-induced stress,” *Shock and Vibration*, vol. 2021, Article ID 5561093, 9 pages, 2021.
- [26] Z. Qin and T. Wang, “Abutment pressure distribution and its transfer law in floor of deep isolated fully-mechanized mining faces using sublevel caving,” *Chinese Journal of Rock Mechanics and Mining Sciences*, vol. 23, no. 7, pp. 1127–1131, 2004.